Metasomatism in the Uppermost Subcontinental Mantle in the Presence of Ti-Rich Hydrous Carbonated Silicate Melt

Naina Goswami[1,✉]

[1] Research School of Earth Sciences, Australian National University, Canberra, Australia

✉ u5960582@anu.edu.au

Keywords: Metasomatism, ultramafic xenoliths, trace elements, carbonatite

1. Introduction

Carbonate-rich melts are characterized by low viscosity and low density (Bodinier et al., 1989; Song and Frey, 1989; Rudnick et al., 1993; Grégoire et al., 2003). These highly mobile primary magmatic liquids have long been recognized as important metasomatic agents altering the mantle geochemistry (Yaxley et al., 1991; Grégoire et al., 2003; Pilet et al., 2016). The origin of carbonatite melts is hypothesized. Hypotheses propose that carbonatite melts are formed either by immiscible separation of parental carbonated silicate magmas at crustal or mantle pressures, crystal fractionation of parental carbonate-silicate magmas and/or low-degree of partial melting of carbonated mantle peridotite below 70 km depth (Yaxley et al., 1991; Yaxley et al., 1998; Pilet et al., 2016; Simandl and Paradis, 2018). Carbonatites can possibly be derived from Earth's crust or mantle with some crustal contribution (e.g. subducted crustal component) (Pilet et al., 2016). Carbonatites and alkaline-carbonatite complex can be emplaced in continental settings (extensional settings related to large-scale intraplate fracture zones), slab windows in subducted plates and in post-collisional orogenic settings, as in British Columbia Alkaline province, Canada (Pell, 1994, Millonig et al., 2012), and the Himalayan collisional zone, western Sichuan, China (Hou et al., 2006). They have also been identified in oceanic island regions, e.g. the Canary Islands, the Cape Verde Islands and the Kerguelen Islands. The commonly observed enrichment in LILE (large-ion lithophile elements) and REEs (rare earth elements) in many peridotite xenoliths hosted by alkali basalts is attributed to cryptic metasomatism by LILE-rich silicate-carbonate fluids (Yaxley et al., 1991; O'Reilly et al., 1991; Dautria et al., 1992) The presence of hydrous phases such as phlogopite and/or pargasite has been attributed to modal metasomatism introduced by Si-undersaturated fluids (Dawson, 1984; Bodinier et al., 1988; Green and Wallace, 1988; Song and Frey, 1989; O'Reilly et al., 1991; Rudnick et al., 1993). Occurrences of such metasomatic episodes have been reported globally (Bodinier et al., 1989; Yaxley et al., 1991; Pilet et al., 2016; Groves et al., 2020; Aulbach et al., 2020). Wallace and Green (1988) first determined experimentally the genesis of the metasomatic melt as a carbonated silica-undersaturated melt generated from the partial melting of periodite + carbonatite + H_2O at varied pressure and temperature conditions. They predicted that a melt with > 40 wt% CO_2 and 1-2 wt% H_2O would be an effective metasomatic agent in transferring LILEs to the upper mantle. Once this melt interacts with the mantle assemblage, it then evolves to a sodic-dolomitic composition (documented as CM1 in Wallace and Green, 1988). Metasomatism of xenoliths by ephemeral carbonate melts leads to the formation of accessory mineral phases like apatites or amphiboles, with simultaneous enrichment in LILEs and REEs in primary clinopyroxenes (Green and Wallace, 1988; Yaxley et al., 1991; Sweeney, 1994; Hammouda and Keshav, 2015). The formation of secondary clinopyroxene and olivine may follow the consumption of orthopyroxene as described by the univariant reaction (Eq. 1)

$$4MgSiO_3 + CaMg(CO_3)_2 = 2Mg_2SiO_4 + CaMgSi_2O_6 + 2CO_2 \quad \textit{(Eq. 1)}$$

$$Orthopyroxene + Dolomite = Olivine + Clinopyroxene + fluid$$

This reaction is controlled by the prevailing mantle conditions i.e. pressure, temperature and redox state. The influx of multiple flows of carbonatitic melts could ultimately lead to the conversion of harzburgite or lherzolitic mantle to orthopyroxene-free wehrlite. These occurrences have been previously documented in peridotite xenoliths (Yaxley et al., 1991; Dautria et al., 1992).

Here we report and investigate first occurrences of carbonate-bearing spinel peridotite xenoliths from a sub-surface Mesozoic basaltic dyke intruding into Palaeozoic granites of Tumut-Eucumbene Tunnel, in Snowy Mountains Region, New South Wales, Australia. To our knowledge, no prior research has been done on the samples recovered from basanite dyke(s) in this region, but numerous studies have investigated the granitic rocks of the area (e.g. Black, 1965; McDougall and Wellman, 1976). This study aims at determining the nature and origin of carbonates by analysing the spinel-peridotite xenoliths from this sample suite and other features they host.

Proceedings of the 5th International YES Congress
DOI: 10.2312/yes19.20

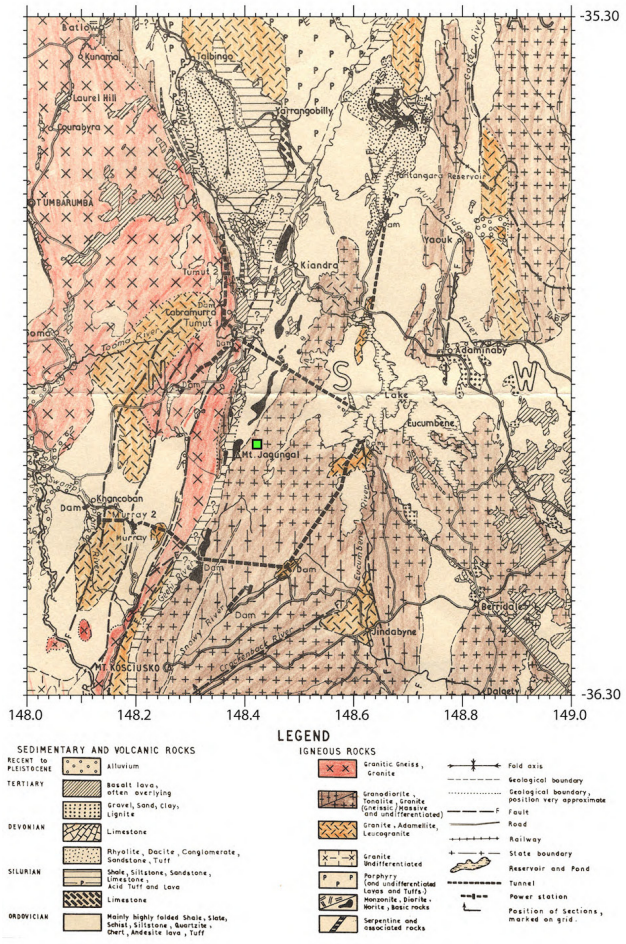

Figure 1: Geological map of Snowy Mountains area highlighting the location of the sampled basanite dyke (modified after Molnar 1963).

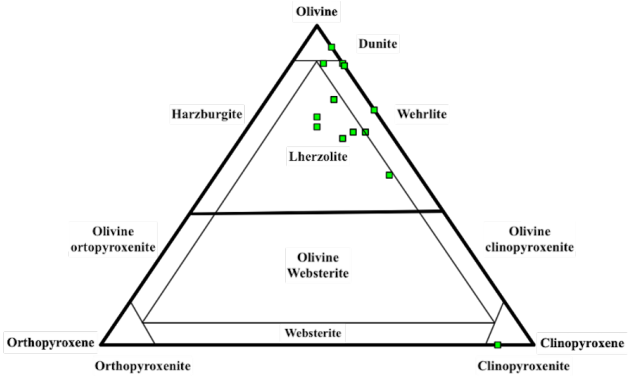

Figure 2: Ternary Diagram describing the modal classification of our suite of xenoliths based on the modal proportions of Olivine (Ol), Orthopyroxene (opx) and Clinopyroxene (cpx).

2. Sample location and Petrography

2.1. Sample location

The samples are spinel lherzolites to wehrlites collected from a sub-surface basanite dyke cutting through the Tumut-Eucumbene Tunnel in Snowy Mountains region, New South Wales, Australia (35.878568° S, 148.420076° E; Fig. 1).

Due to the subsequent flooding of Lake Eucumbene in 1958, any opportunity of further sampling was lost, thus making these samples novel. This intrusion was mapped to be about 2.5 m across and composed of massive, fine-grained alkaline basalt enveloping rounded inclusions of peridotite. The matrix basalt was texturally very similar to the Tertiary flows of the area and was assumed to be associated with the Monaro Volcanics. K-Ar ages on whole-rock from this dyke gave an age of 168 ± 7 Ma (McDougall and Wellman, 1976), similar to the ages of the igneous units in Cooma region.

2.2. Petrography

Petrographically, the samples are a suite of ultramafic spinel peridotites ranging from lherzolitic to wehrlitic mineralogy (Fig. 2).

The samples consist of neoblasts and porphyroblasts of olivine + clinopyroxene + spinel ± orthopyroxene. The majority of these samples are devoid of orthopyroxene along with concomitant presence of apatite, amphibole and patches of carbonate. Minor proportions of apatite, sulphide and ilmenite precipitates are also found. Chemical equilibrium between the minerals and matrix in the samples is reasonably assumed from absence of compositional zoning in the minerals. The mineral grains in the entire suite are heavily fractured by basanite melt veins, carbonate patches and serpentine mesh, producing a range of textures.

3. Analytical Methods

Major element compositions of our samples were analysed using the electron probe micro analyser CAMECA SX-100 and JEOL 8310 at the Research School of Earth Sciences (RSES) and the Centre for Advanced Microscopy (CAM), respectively, at Australian National University (ANU). All analyses were operated with an accelerating voltage of 15 kV, a beam current of 20 nA, and beam diameters varying between 1 µm and 5 µm with a counting time of 10 to 30 s. A minimum of 3 analyses per grain was performed on each sample.

Along with major elements, trace element compositions were also analysed in these samples with laser ablation mass spectrometry using the single collector ICP-MS Agilent 7700 coupled with the ArF EXCIMER laser (193 nm wavelength, 20 ns pulse width, 103 µm diameter) at RSES, ANU. Polished thin sections (50 to 100 µm thick) were ablated to carry out spot analyses using NIST SRM-610 as calibration standard and NIST SRM-612 and BCR-2g as secondary standards. A 81 µm spot size was used for clinopyroxene and amphibole analyses. The analyses followed the “sandwich method” i.e. the sample analyses (7 to 8

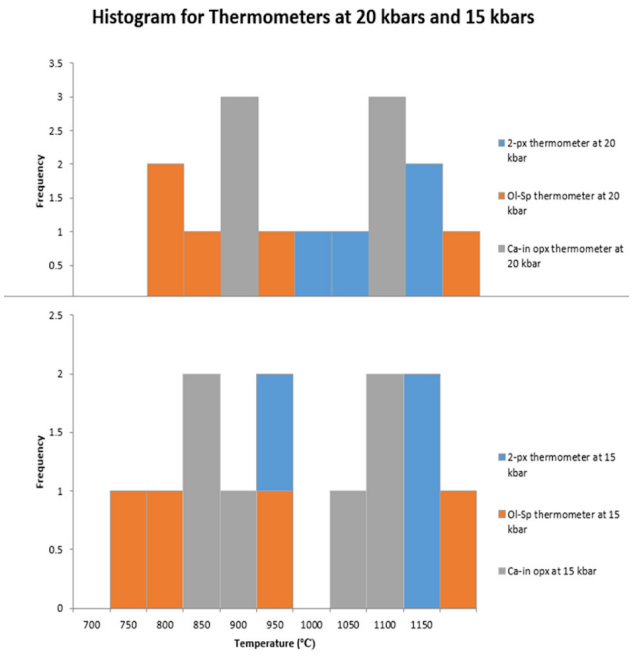

Figure 3: Histogram of equilibration temperatures estimated for the sample suite at 20 kbars (top) and 15 kbars (bottom), as calculated from various experimentally-derived thermometers (2-pyroxene and Ca-in-orthopyroxene methods from Brey and Köhler (1990); olivine-spinel method from Balhaus et al. (1990)).

analyses per sample) were bracketed between the secondary standards. Clinopyroxene and amphiboles trace element data was reduced using ^{43}Ca concentrations.

4. Thermometry

Equilibration temperatures (°C) for our xenoliths were calculated using 3 different thermometers based on cation exchange in/between minerals at 15 and 20 kbars (assumed representative pressures for spinel peridotite facies).

4.1. Ca-in orthopyroxene thermometer

Temperatures were calculated using Ca content in orthopyroxene (Ca-in-opx) as a thermometer using the formula given by Brey and Köhler (1990).

4.2. Two-pyroxene thermometer

Temperatures were also calculated employing the two-pyroxene thermometer based on the partitioning of Ca between orthopyroxene and clinopyroxene given by Brey and Köhler (1990).

4.3. Olivine-Spinel Fe-Mg exchange thermometry

Temperatures were also calculated using exchange of Fe and Mg between olivine and spinels given by Balhaus et al. (1991).

4.4. Calculation of ferric ion (Fe^{3+}) in spinels

Fe^{3+} content of spinel was calculated using a simple equation by Droop (1987) in ferromagnesian oxides and silicates using microprobe analyses assuming perfect stoichiometry. This equation has been derived assuming stoichiometric criteria where iron is the only element with a variable valency and oxygen is the only present anion. The equation (Eq. 2) is given as

$$F = 2X\left(1 - \frac{T}{S}\right) \qquad \textit{(Eq. 2)}$$

Here, F is the number of Fe^{3+} per X number of oxygen ions in a mineral formula. T is the ideal number of cations per formula unit, and S corresponds to the observed cation total for X oxygen ions assuming all iron to be Fe^{2+}.

4.5. Oxygen Fugacity

Oxygen fugacity f_{O2} was calculated using data obtained from the Olivine-spinel thermometer of Balhaus et al. (1991), and is calculated relative to FMQ (Fayalite-Magnetite-Quartz) buffer. The estimates were found to be ± 1.5 log units relative to FMQ. The element concentrations were obtained from microprobe analyses using Eq. 3:

$$\Delta log(fO)_2^{FMQ} = 0.27 + \frac{2505}{T} - \frac{400P}{T} - 6\log(X_{Fe}^{olv}) - \frac{3200(1 - X_{Fe}^{Olv})^2}{T} + 2\log\left(X_{Fe^{2+}}^{Sp}\right) + 4\log\left(X_{Fe^{3+}}^{Sp}\right) + \frac{2630\left(X_{Al}^{Sp}\right)^2}{T} \qquad \textit{(Eq. 3)}$$

where Fe^{3+}, Fe, Fe^{2+} and Al are the respective concentrations in spinels and olivines to calculate the molar ratio *X*, *P* is the assumed pressure in GPa and *T* the temperature calculated from the Fe-Mg olivine-spinel exchange thermometer in K.

5. Discussion

5.1. Equilibration Conditions

Temperatures calculated using various thermometers are consistent with those expected for spinel lherzolite facies in the upper mantle. The temperatures calculated using the above thermometers are within ± 50°C of each other at 15 and 20 kbars and range from 800°C to 1200°C, and are thus reasonable for samples to be spinel lherzolites facies (Fig. 3). The differences in temperature estimates from the Ca-in-opx and the 2-pyroxene thermometer are higher at 15 kbars than at 20 kbars. The reason for $T_{Ca\text{-}in\text{-}opx} > T_{2\text{-}px}$ could be attributed to calibration errors but could also be theoretically inferred from the shape of the miscibility gap in the orthopyroxene-clinopyroxene phase diagram (Balhaus et al., 1991). The Ca-in-opx thermometer becomes more sensitive and hence reliable at low temperatures, while 2-pyroxene thermom-

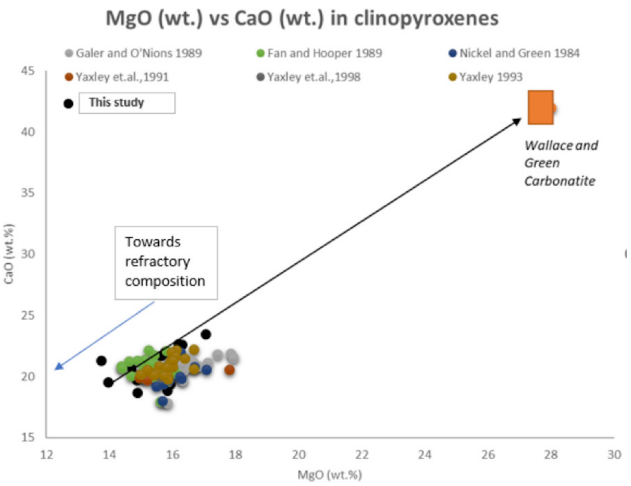

Figure 4: Plot of MgO vs CaO for clinopyroxene in spinel peridotite. Note the mixing relationship between a pure carbonatite melt (Wallace and Green, 1988) and pre-metasomatic lithosphere to generate the carbonatized xenoliths and enrichment in CaO concentrations.

eter is sensitive and reliable at higher temperatures (Balhaus et al., 1991). The temperatures calculated using Fe-Mg exchange olivine-spinel thermometry are reasonable estimates and are within ± 100°C of the other thermometers. Differences in temperature estimates from this thermometer could be ascribed to systematic errors in calculating $Fe^{3+}/\sum Fe$.

5.2. Evidence for Metasomatism

5.2.1. Major Elements

Olivines in the sample suite have Mg# (molar Mg/(Mg+Fe)) ranging from 85.04 to 90.06 and averaging to 87.75, typical for primitive peridotites.

Clinopyroxenes from this suite exhibit increasing CaO and P_2O_5 trends with increasing MgO, while Al_2O_3 and SiO_2 decrease. These diminutions could be indicative of adding a component to these xenoliths at depth, which is substantially rich in CaO and P_2O_5 and depleted in Al and Si. This interpretation is consistent with a metasomatic process involving the uptake of components by refractory lithosphere being dolomitic, Si-undersaturated, phosphate-rich and accompanied by a substantial loss of a CO_2-rich fluid during ascent (Fig. 4).

5.2.2. Trace Elements

In this study, clinopyroxenes have subchondritic Y/Ho, Ti/Eu, Nb/La and Nb/Ta ratios with superchondritic Zr/Hf ratios. Amphiboles are major hosts for Nb and Ti along with Ta. Nb/Ta in xenoliths is a metasomatic signature or a consequence of Ti-oxide fractionation. $(La/Yb)_N$ (N = mantle normalized) in the clinopyroxenes range from 2.10 to 5.35, averaging to 3.35. This dominant $(La/Yb)_N > 1$ in xenoliths is consistent with a commonly held view of widespread metasomatic effect on lithosphere (Kalfoun and Merlet, 2002).

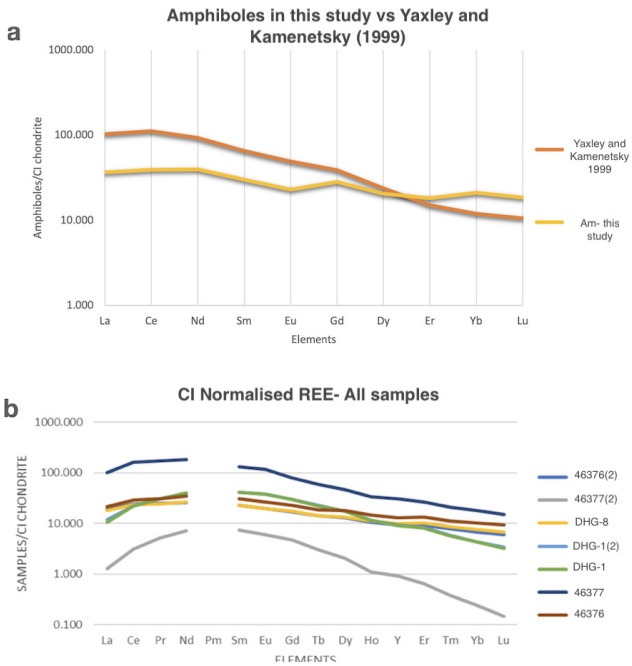

Figure 5: CI chondrite normalized plot for (a) amphiboles from this study and in Yaxley and Kamenetsky (1999) and (b) clinopyroxenes from this study.

The amphiboles from this study are richer in HREE compared to amphiboles from those in Yaxley and Kamenetsky (1999) (Fig. 5).

5.3. Nature of Metasomatic Process

The spinel peridotites equilibrated at assumed pressures of 15 and 20 kbars (for spinel peridotite facies) are metasomatised and are suggestive of a two-stage metasomatic process:

The first stage is the precipitation of hydrous phases (amphiboles ± phlogopite) which may be related to

$$orthopyroxene\ (P) + Al\text{-}spinel\ (P) + Cr\text{-}diopside\ (P) + fluid = amphibole\ (P) + phlogopite\ (P) + Al\text{-}Cr\text{-}spinel\ (S) + olivine\ (S) \quad \textit{(Eq. 4)}$$

Eq. 4, obtained from Dautria et al. (1992):

where *P* and *S* are primary and secondary mineral lithologies, respectively. This reaction would require the fluid to be H_2O- rich and high in Na, K, Ti and Fe. Such a fluid could be a silicate melt of alkali basaltic composition.

The second stage is characterized by the percolation of a sodic-dolomitic melt reacting with orthopyroxene producing secondary olivine, clinopyroxene and carbonates (calcite + magnesite), represented through Eq. 1.

This leads to the decarbonation of the carbonatite melt and transformation of the whole rock mineralogy from spinel lherzolite to orthopyroxene-free spinel wehrlite. During this process, other components of the carbonatite (Ti, P, K, Na, H_2O) contribute to the precipitation of Ti-rich amphiboles, phlogopites and apatites.

6. Summary

The study of spinel peridotites from a basanite dyke in Tumut-Eucumbene tunnel highlights their primitive origin and fertile nature. The presence of a variety of primary and secondary mineral assemblages in these samples is indicative of a fluid event. Elemental analyses of clinopyroxenes and amphiboles hints at a metasomatic process where interaction of LILE-rich carbonatite melt exhausted most of the orthopyroxene within the sample suite precipitating new secondary mineral phases. Such events have been commonly documented globally, especially in Western Victoria, Australia (Yaxley et al., 1991, Yaxley et al., 1998). Based on textural and element analyses, a metasomatic model is proposed in this study, where the consumption of orthopyroxene by carbonatite melts at ~15 to 20 kbars is accompanied by the precipitation of secondary amphibole, phlogopite, Al-Cr-spinel and olivine. This reaction follows the early precipitation of hydrous phases such as amphibole and/or phlogopite at the expense of primary orthopyroxene, Al-spinel and Cr-diopside on reacting with a hydrous, alkali and LILE-rich silicate carbonated melt. Such fluids have been envisaged as metasomatic agents in the past, hinting at the vast LILE- and carbonate-rich budget of the mantle. This has implications on the nature of fluids/melts involved and their genesis. The usage of approximated pressure values in this study opens up the possibility to evaluate them precisely. This study encourages to analyse in detail the mechanisms involved in metasomatism and understand them more precisely. It would be useful to look for water concentrations in mineral phases to identify the role of the hydrous mantle aiding in the precipitation of hydrous minerals, and its effects on the process of partial melting. Analyzing $\delta^{13}C$ and $\delta^{18}O$ of carbonates could assist in establishing the source of carbonates – whether they are subducted sedimentary carbonates or sourced at depth in earth's mantle.

7. Acknowledgement

I would like to thank Greg Yaxley (supervisor), Marnie Forster, and Thomas Rose for their endless support.

8. References

Aulbach, S., Viljoen, K.S., Gerdes, A., 2020. Diamondiferous and barren eclogites and pyroxenites from the western Kaapvaal craton record subduction processes and mantle metasomatism, respectively. Lithos 368-369, 105588. https://doi.org/10.1016/j.lithos.2020.105588.

Balhaus, C., Berry, R. F., Green, D. H., 1991. Oxygen fugacity controls in the Earth's upper mantle. Nature 348, pp. 437–440. https://doi.org/10.1038/348437a0.

Black, P., 1965. Geology of the Eucumbene Area. Canberra, Australian National University, unpublished BSc (Hons) thesis.

Bodinier, J.-L., Dupuy, C., Dostal, J., 1988. Geochemistry and petrogenesis of Eastern Pyrenean peridotites. Geochimica et Cosmochimica Acta 52, pp. 2893–2907. https://doi.org/10.1016/0016-7037(88)90156-1.

Bodinier, J.-L., Vasseur, G., Vernierres, J., Dupuy, C., Fabries, J., 1989. Mechanims of Mantle Metasomatism: Geochemical Evidence from the Lherz Orogenic Peridotite. Journal of Petrology 31(3), pp. 597–628. https://doi.org/10.1093/petrology/31.3.597.

Brey, G. P., Köhler, T., 1990. Geothermobarometry in Four-phase Lherzolites II. New Thermobarometers, and Practical Assessment of Existing Thermobarometers. Journal of Petrology 31(6), pp. 1353–1378. https://doi.org/10.1093/petrology/31.6.1353.

Dautria, J. M., Dupuy, C., Takherist, D., Dostal, J., 1992. Carbonate metasomatism in the lithospheric mantle: peridotitic xenoliths from a melilitic district of the Sahara Basin. Contributions to Mineralogy and Petrology 111(1), pp. 37–52. https://doi.org/10.1007/BF00296576.

Dawson, J. B., 1984. Contrasting Types of upper-Mantle Metasomatism? Developments in Petrology 11(2), pp. 289–294. https://doi.org/10.1016/B978-0-444-42274-3.50030-5.

Droop, G. T., 1987. A general equation for estimating Fe^{3+} concentrations in ferromagnesian silicates and oxides from microprobe analyses, using stoichiometric criteria. Mineralogical Magazine 51(361), pp. 431–435. https://doi.org/10.1180/minmag.1987.051.361.10.

Green, D. H., Wallace, M. E., 1988. Mantle metasomatism by ephemeral carbonatite melts. Nature 336, pp. 459–462. https://doi.org/10.1038/336459a0.

Grégoire, M., Bell, D. R., Le Roex, A. P., 2003. Garnet Lherzolite from the Kaapvaal Craton (South Africa): Trace Element Evidence for a Metasomatic History. Journal of Petrology 44(4), pp. 629–657. https://doi.org/10.1093/petrology/44.4.629.

Groves, D. I., Zhang, L., Santosh, M., 2020. Subduction, mantle metasomatism, and gold: A dynamic and genetic conjunction. Geological Society of America Bulletin 132(7-8), pp. 1419–1426. https://doi.org/10.1130/B35379.1.

Hammouda, T., Keshav, S., 2015. Melting in the mantle in the presence of carbon: Review of experiments and discussion on the origin of carbonatites. Chemical Geology 418, pp. 171–188. https://doi.org/10.1016/j.chemgeo.2015.05.018.

Hou, Z., Tian, S., Yuan, Z., Xie, Y., Yin, S., Yi, L., Fei, H., Yang, Z., 2006. The Himalayan collision zone carbonatites in western Sichuan, SW China: Petrogenesis, mantle source and tectonic implication. Earth and Planetary Science Letters 244(1-2), pp. 234–250. https://doi.org/10.1016/j.epsl.2006.01.052.

Kalfoun, I. D., Merlet, C., 2002. HFSE residence and Nb/Ta ratios in metasomatised, rutile-bearing mantle peridotites. Earth and Planetary Science Letters 199(1-2), pp. 49–65. https://doi.org/10.1016/S0012-821X(02)00555-1.

McDougall, I., Wellman, P., 1976. Potassium-Argon ages for some Australian Mesozoic Igenous Rocks. Journal of the Geological Society of Australia 23, pp. 1–9. https://doi.org/10.1080/00167617608728916.

Millonig, L. J., Gerdes, A., Groat, L. A., 2012. U–Th–Pb geochronology of meta-carbonatites and meta-alkaline rocks in the southern Canadian Cordillera: A geodynamic perspective. Lithos 152(1), pp. 202–217. https://doi.org/10.1016/j.lithos.2012.06.016.

Molnar, A., 1963. Geological Map of Snowy Mountains Area. Cooma, Snowy Mountains Hydro electric authority. http://hdl.handle.net/11343/23948.

O'Reilly, S. Y., Griffin, W. L., Ryan, C. G., 1991. Residence of trace elements in metasomatised spinel lherzolite xenoliths: a proton-microprobe study. Contributions to Mineralogy and Petrology 109, pp. 98–113. https://doi.org/10.1007/BF00687203.

Pell, J., 1994. Carbonatites, Nepheline syenites, Kimberlites and related rocks; in British Columbia, Bulletin (British Columbia. Ministry of Energy, Mines and Petroleum Resources) 88, 136 p. [online] Available at: http://cmscontent.nrs.gov.bc.ca/geoscience/PublicationCatalogue/Bulletin/BCGS_B088.pdf [Accessed 21 November 2020].

Pilet, S., Abe, N., Rochat, L., Kaczmarek, M.-A., Hirano, N., Machida, S., Buchs, D. M., Baumgartner, P. O., Müntener, O., 2016. Pre-subduction metasomatic enrichment of the oceanic lithosphere induced by plate flexure. Nature Geoscience 9, pp. 898–903. https://doi.org/10.1038/ngeo2825.

Rudnick, R. L., McDonough, W. F., Chappell, B. W., 1993. Carbonatite metasomatism in the northern Tanzanian mantle: petrographic and geochemical characteristics. Earth and Planetary Science Letters 114, pp. 463–475. https://doi.org/10.1016/0012-821X(93)90076-L.

Simandl, G. J., Paradis, S., 2018. Carbonatites: related ore deposits, resources, footprint, and exploration methods, Applied Earth Science 127(4), pp. 123–152. https://doi.org/10.1080/25726838.2018.1516935.

Song, Y., Frey, F. A., 1989. Geochemistry of peridotite xenoliths in basalt from Hannuoba, Eastern China: Implications for subcontinental mantle heterogeneity. Geochimica et Cosmochimica Acta 53(1), pp. 97–113. https://doi.org/10.1016/0016-7037(89)90276-7.

Sweeney, R. J., 1994. Carbonate melt compositions in the Earth's mantle. Earth and Planetary Science Letters 128, pp. 259–270. https://doi.org/10.1016/0012-821X(94)90149-X.

Wallace, M. E., Green, D. H., 1988. An experimental determination of primary cabonatite magma composition. Nature 335, pp. 343–346. https://doi.org/10.1038/335343a0.

Yaxley, G. M., Crawford, A. J., Green, D. H., 1991. Evidence for carbonatite metasomatism in spinel peridotite xenoliths from western Victoria, Australia. Earth and Planetary Science Letters 107(2), pp. 305–317. https://doi.org/10.1016/0012-821X(91)90078-V.

Yaxley, G. M., Green, D. H., Kamenetsky, V., 1998. Carbonatite Metasomatism in the Southeastern Australian Lithosphere. Journal of Petrology 39, pp. 1917–1930. https://doi.org/10.1093/petroj/39.11-12.1917.

Yaxley, G. M., Kamenetsky, V., 1999. In situ origin for glass in mantle xenoliths from southeastern Asutralia: insights from trace element compositions of glasses and metasomatic phases. Earth and Planetary Science Letters 172(1-2), pp. 97-109. https://doi.org/10.1016/S0012-821X(99)00196-X.